Carbon isotopic excursions and detailed ammonoid and conodont biostratigraphies around Smithian–Spathian boundary in the Bac Thuy Formation, Vietnam

Toshifumi Komatsu [a,*], Reishi Takashima [b], Yasunari Shigeta [c], Takumi Maekawa [a], Huyen Dang Tran [d], Tien Dinh Cong [d], Susumu Sakata [e], Hung Doan Dinh [f], Osamu Takahashi [g]

[a] Graduate School of Science and Technology, Kumamoto University, Kumamoto 860-8555, Japan
[b] The Center for Academic Resources and Archives Tohoku University Museum, Tohoku University, Aramaki Aza Aoba 6-3, Aoba-ku, Sendai 980-8578, Japan
[c] Department of Geology and Paleontology, National Museum of Nature and Science, 4-1-1 Amakubo, Tsukuba 305-0005, Japan
[d] Vietnam Institute of Geosciences and Mineral Resources (VIGMR), Hanoi, Viet Nam
[e] Institute for Geo-Resources and Environment, National Institute of Advanced Industrial Science and Technology (AIST), 1-1-1 Higashi, Tsukuba 305-8567, Japan
[f] Vietnam National Museum of Nature (VNMN), Hanoi, Viet Nam
[g] Department of Astronomy and Earth Sciences, Tokyo Gakugei University, Koganei, Tokyo 184-8501, Japan

ABSTRACT

The Smithian–Spathian boundary is indicated by the first occurrence of the ammonoid *Tirolites* cf. *cassianus* in the Olenekian Bac Thuy Formation, northeastern Vietnam. The boundary is intercalated within organic-rich dark gray mudstone that accumulated under anoxic to dysoxic conditions in the An Chau and Nanpanjiang Basins on the South China Block. In Lang Son area, three conodont zones, *Novispathodus* ex gr. *waageni*, *Novispathodus* ex gr. *pingdingshanensis*, and *Icriospathodus collinsoni*, are recognized in the formation. The Smithian–Spathian boundary is intercalated within *N*. ex gr. *pingdingshanensis* conodont Zone. The positive excursion in $\delta^{13}C$ with values increasing from around $-2.3‰$ to $+5.7‰$ was recorded in the uppermost Smithian *Xenoceltites variocostatus* ammonoid beds and *N*. ex gr. *pingdingshanensis* conodont Zone. The $\delta^{13}C$ values decrease across the Smithian–Spathian boundary. These $\delta^{13}C$ isotopic patterns are correlated with well-known positive excursions around the Smithian–Spathian boundary globally.

© 2016 Elsevier B.V. All rights reserved.

1. Introduction

Around the Smithian–Spathian (S–S), mid Olenekian boundary in the Early Triassic, drastic change of marine ecosystems are recognized as significant in delaying recovery of marine fauna following the end-Permian mass extinction (Galfetti et al. 2007; Algeo et al. 2011; Payne and Clapham 2012; Sun et al. 2012). At that time, an intense ocean anoxic event characterized by the accumulation of organic-rich black shale, a decrease in U/Th and ΩCe of conodont teeth and pyrite framboid size distributions has been reported (Galfetti et al. 2008; Song et al. 2012; Komatsu et al. 2014a; Shigeta et al. 2014; Tian et al. 2014). The resulting positive carbon isotope excursion is associated with global climate change in both marine and terrestrial ecosystems (Payne et al. 2004; Galfetti et al. 2007, 2008; Horacek et al. 2007; Tong et al. 2007; Saito et al. 2013). These climatic changes and fluctuations of marine productivity had an influence on the global patterns of ammonoid distribution, and dampened the radiations of ammonoid and conodont faunas in the latest Smithian (Galfetti et al. 2007, 2008; Orchard 2007; Stanley 2009).

The Smithian–Spathian boundary is generally defined by ammonoid and conodont biostratigraphic zones, although the boundary of GSSP isn't designated. The basal Spathian is marked by the appearance of many new ammonoid taxa, including dinaritines, tirolitines and columbitids (Balini et al. 2010); *Tirolites* in particular is a significant age diagnostic ammonoid in the lowest Spathian (Galfetti et al. 2008; Ogg 2012; Shigeta et al. 2014). Among conodonts, the first appearance of *N. pingdingshanensis* (= *N. pingdingshanensis* in Goudemand et al. 2012) has been used as a guide to the S–S boundary in south China (Zhao et al. 2007; Tong et al. 2007; Liang et al. 2011; Chen et al. 2013, 2015). Payne et al. (2004) and Song et al. (2012) correlated south Chinese sections and carbon isotopic excursions on the basis of first appearance of *Neospathodus crassatus* (= *Icriospathodus*? *crassatus* in Orchard 1995).

We recovered abundant collections of ammonoids and conodonts, including the basal Spathian age diagnostic species, in the Olenekian
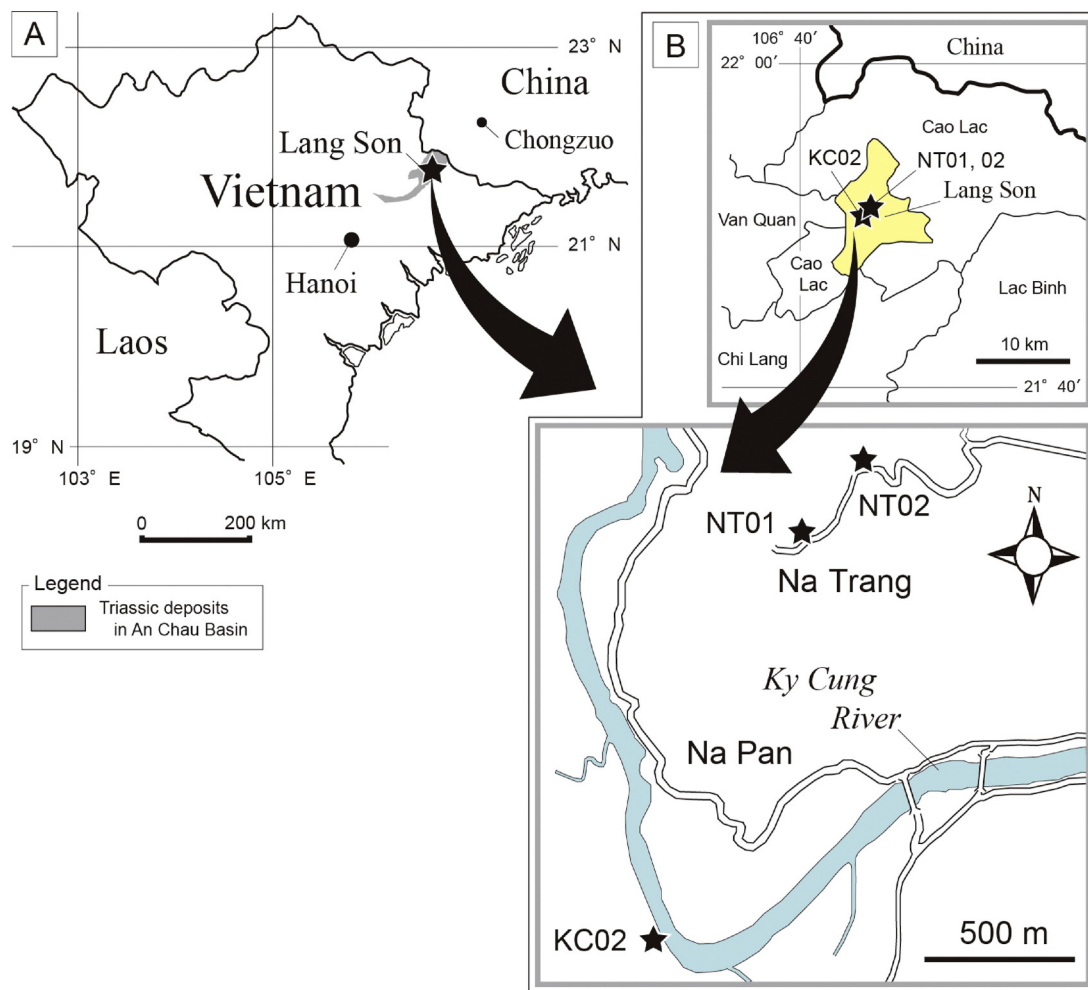
Fig. 1. (A) Map showing the An Chau Basin located primarily in Lang Son Province, Vietnam. (B) Location of the study area. Black stars representing the locations of the studied sections (NT01, KC02).

sections of northeastern Vietnam (Fig. 1; Shigeta et al. 2014). In this study, we report additional collections of ammonoid and conodont specimens from the middle part of the Bac Thuy Formation, and calibrate detailed ammonoid and conodont biostratigraphic data and carbon isotopic excursions around the S–S boundary. The total organic carbon content (TOC) from the latest Smithian to earliest Spathian organic-rich dark-gray limestone and black mudstone was also measured.

2. Geologic setting

In the An Chau Basin of Vietnam (Fig. 1), the Lower Triassic is composed of siliciclastics of the Induan to lower Olenekian Lang Son Formation, and the Olenekian Bac Thuy Formation characterized by carbonates (Dang and Nguyen 2005; Komatsu and Dang 2007; Maekawa et al. 2015). The Bac Thuy Formation is approximately 40 to 200 m in thickness (Dang 2006; Komatsu et al. 2014a; Shigeta et al. 2014; Maekawa et al. 2016), and consists mainly of fossiliferous carbonates, limestone breccia, and hemipelagic basinal marl and mudstone (Fig. 2). This formation conformably overlies the Lang Son Formation, and is unconformably overlain by the Middle Triassic (Anisian–Ladinian) Khon Lang Formation, which consists mainly of volcanic and siliciclastic rocks (Dang 2006; Shigeta et al. 2014).

In the Lang Son area (Fig. 1), the Bac Thuy Formation is divided into lower, middle and upper parts, and is characterized by a typical

transgressive succession ranging from tide- and wave-influenced shallow marine carbonate platform, through slope, and finally marginal basin plain environments (Komatsu et al. 2014a).

The lower part of the formation consists mainly of thick limestone breccia, bedded limestone, thin-bedded lime mudstone, and hemipelagic greenish gray mudstone. Thin shallow marine carbonate platform deposits crop out along a tributary of the Ky Cung River near Na Pan (Fig. 1, section KC01 in Komatsu et al. 2014a; Shigeta et al. 2014). The bioclastic shallow marine platform limestone and slope deposits of the lower Bac Thuy Formation commonly yield early Olenekian (Smithian) ammonoids *Owenites koeneni* and *Submeekoceras hsüyüchieni* (Shigeta et al. 2014).

The middle part of the Bac Thuy Formation is characterized by alternating dark gray organic-rich limestone and mudstone yielding abundant radiolarians, the bivalve *Crittendenia*, the uppermost Smithian ammonoid *Xenoceltites variocostatus*, and the lowermost Spathian *Tirolites* cf. *cassianus* (Komatsu et al. 2013, 2014a; Shigeta et al. 2014). Komatsu et al. (2014a) reported that the Smithian–Spathian boundary, which embedded in anoxic to dysoxic facies characterized by organic-rich mudstone, is intercalated in the middle part of the formation.

The upper part of the Bac Thuy Formation is dominated by thick greenish gray hemipelagic mudstone intercalating with thin calciturbidite layers, bedded limestones, and limestone breccias. The
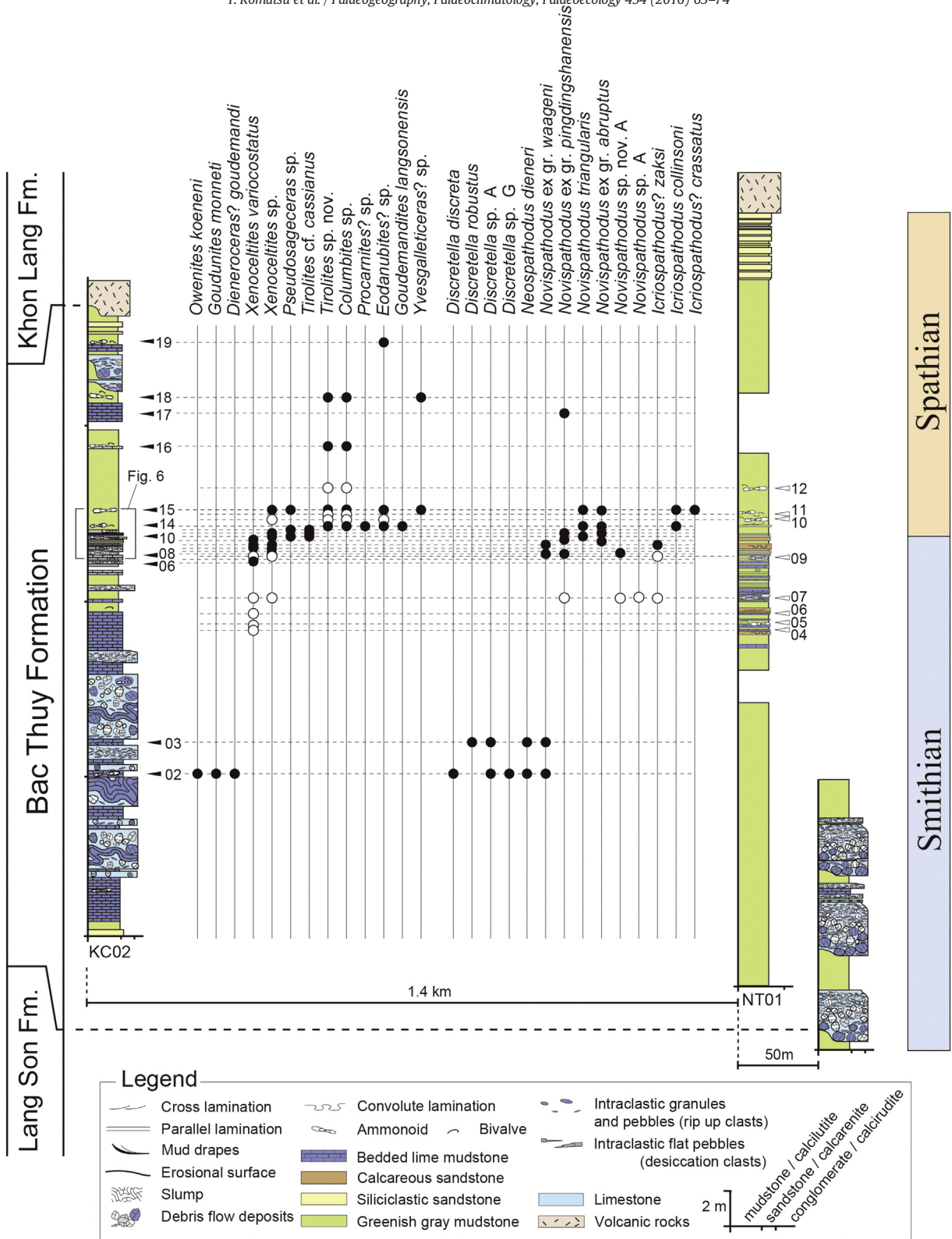
Fig. 2. Columnar sections of the Bac Thuy Formation and distributions of ammonoids and conodonts in NT01 (open circles) and KC02 (solid dots). Typical forms of *N. pingdingshanensis* occur from KC02-10 and NT01-07.

mudstone is locally overlain by alternating siliciclastic sandstone and mudstone. The hemipelagic mudstone and calciturbidite layers commonly contain Spathian ammonoids *Columbites* and *Tirolites,* and the bivalves *Crittendenia, Leptochondria,* and *Bositra.* These thick mudstones may have accumulated in marginal basin plain environments (Komatsu et al. 2014a).

The Lower Triassic deposits of the An Chau Basin extend into the southern Nanpanjiang Basin in South China, which was filled with mudstones and debris flow deposits of the Induan to Olenekian Luolou Formation, and with shallow marine isolated platform deposits of the Induan Majiaoling Formation, and the Induan to Olenekian Beisi Formation (Enos et al. 2006; Lehrmann et al. 2007a,b). The Bac Thuy
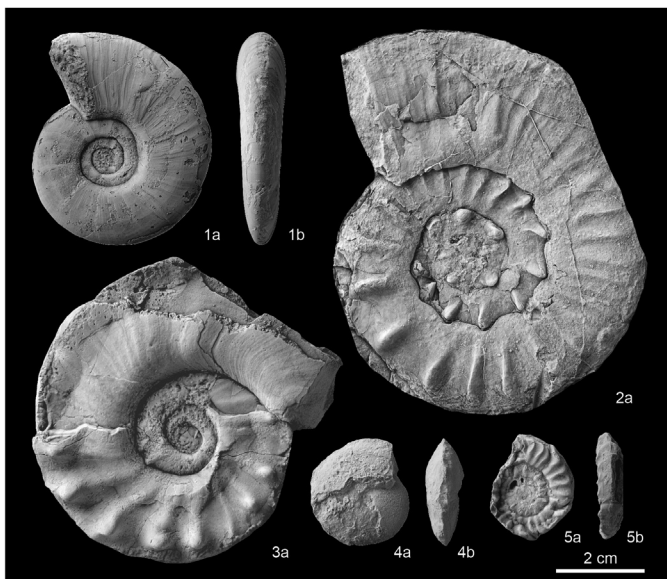
Fig. 3. Age diagnostic ammonoids from the middle part of the Bac Thuy Formation, Lang Son area, northeastern Vietnam. NMNS = National Museum of Nature and Science, Tsukuba. Figures "a" and "b" show lateral and ventral views of specimens, respectively. 1, *Xenoceltites variocostatus* Brayard & Bucher, NMNS PM23479, from NT01-07. *Tirolites* cf. *cassianus* (Quenstedt), NMNS PM23664, from KC02-12. 3, *Tirolites* sp. nov., NMNS PM23668, from KC02–14. 4, *Owenites koeneni* Hyatt and Smith, NMNS PM23582, from KC01-11. 5, *Columbites* sp., NMNS PM23700, from KC02-14.

Formation is lithologically equivalent to the Luolou Formation (Komatsu et al. 2014a).

3. Methods and studied sections

We investigated along the Ky Cung River (section KC02 in Komatsu et al. 2014a; Shigeta et al. 2014) in western Lang Son City and in Na Trang village (section NT01 in Komatsu et al. 2014a; Shigeta et al. 2014), central Lang Son City. Section KC02 is approximately 1.4 km far from section NT01.

In KC02, the age diagnostic basal Spathian ammonoid *T.* cf. *cassianus* was found in dark gray mudstone in the middle part of the Bac Thuy Formation (Figs. 2-4), and the lower Spathian ammonoid assemblage characterized by *Tirolites* sp. nov. was found in carbonate layers 25 cm higher than mudstone beds yielding *T.* cf. *cassianus*. The *Tirolites* sp.
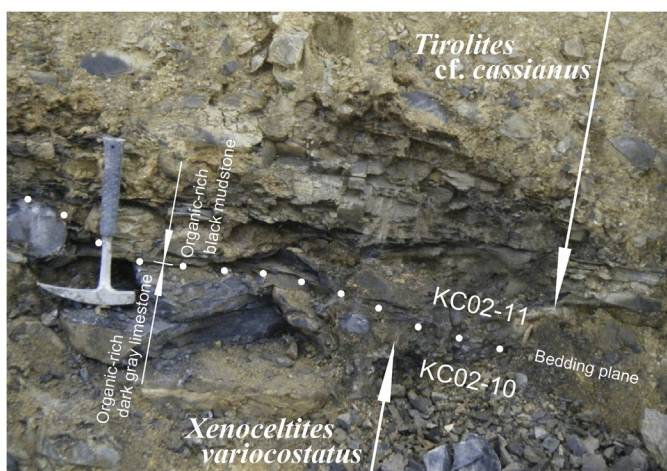
Fig. 4. Photo showing outcrop view of Smithian–Spathian boundary as defined by the first occurrence (FO) of the Spathian index ammonoid *Tirolites* cf. *cassianus* intercalated within the organic-rich black mudstone.

nov. ammonoid assemblages are commonly found in the carbonate layers in the middle and upper parts of the Bac Thuy Formation in ections KC02 and NT01, and these sections are correlated by the first occurrence of *Tirolites* sp. nov. Limestone specimens (C01-25 and T01-12) from both the KC02 and NT01 sections were sampled for carbon isotope analysis (Table 1).

The oxygen and carbon isotope of bulk carbonate of limestone and marl were analyzed with GVI Isoprime Dual Inlet coupled to a Multiprep at GNS Science, New Zealand. 1 mg of powdered samples was reacted with 100% phosphoric acid at 50 °C. Three laboratory carbonate standards calibrated against VPDB were run in each set of analysis and NBS19 once every three or four analysis runs. The internal precision is 0.03% and 0.06% (1σ) for $\delta^{13}C$ and $\delta^{18}O$, respectively.

For the TOC analysis, powdered samples were weighed on ceramic boats, and 1 N HCl was pipetted into each sample boat until carbonate was entirely removed. The samples were then heated at 80 °C for at least 6 h to drive off HCl and water before analysis with the Yanako MT-5 CHN analyzer at the Geological Survey of Japan laboratory with combustion at 950 °C for 5 min. Hippuric acid was used as standard for CHN calibration. Results of duplicate analyses were confirmed to be identical within 5%.

4. Biostratigraphy

4.1. Ammonoid biostratigraphy

The Ammonoid biostratigraphy of the Bac Thuy Formation was reported by Shigeta et al. (2014). According to Shigeta et al. (2014), four ammonoid beds, *O. koeneni*, *X. variocostatus*, *T.* cf. *cassianus*, and

Table 1
Carbon isotopic data from sections NT01, NT02 and KC02.

Section	Sample	$\delta^{13}C_{carbonate}$ (‰)	Rock
KC02	C01	−2.34	White limestone
KC02	C02	−2.29	White limestone
KC02	C03	−2.36	White limestone
KC02	C04	−2.40	White limestone
KC02	C05	−2.29	White limestone
KC02	C06	−2.27	White limestone
KC02	C07	−2.47	White limestone
KC02	C08	−2.18	White limestone
KC02	C09	−0.81	Gray limestone
KC02	C10	−1.17	Gray limestone
KC02	C11	−1.38	Gray limestone
KC02	C12	5.02	Dark gray limestone
KC02	C13	5.74	Dark gray limestone
KC02	C14	5.14	Dark gray limestone
KC02	C15	5.45	Dark gray limestone
KC02	C16	4.51	Dark gray limestone
KC02	C17	5.36	Dark gray limestone
KC02	C18	5.05	Dark gray limestone
KC02	C19	5.03	Dark gray limestone
KC02	C20	4.76	Dark gray limestone
KC02	C21	1.31	Gray limestone
KC02	C22	1.57	Gray limestone
KC02	C23	2.05	Gray limestone
KC02	C24	1.88	Gray limestone
KC02	C25	2.14	Gray limestone
NT02	T01	−1.92	White limestone
NT02	T02	−2.07	White limestone
NT02	T03	−2.24	White limestone
NT01	T04	−2.49	Gray limestone
NT01	T05	−2.22	Gray limestone
NT01	T06	−0.86	Dark gray limestone
NT01	T07	0.26	Dark gray limestone
NT01	T08	4.29	Dark gray limestone
NT01	T09	4.74	Dark gray limestone
NT01	T10	5.07	Dark gray limestone
NT01	T11	5.64	Dark gray limestone
NT01	T12	5.51	Dark gray limestone

Tirolites sp. nov. beds, were recognized in the Ky Cung River sections (sections KC01–02).

O. koeneni has been reported from all over the world, and is regarded as an important middle Smithian index ammonoid (ex. Kiparisova and Popov 1956; Brayard and Bucher 2008; Balini et al. 2010). *X. variocostatus* ammonoid beds are recognized as indicating the uppermost Smithian in Vietnam (Shigeta et al. 2014), because the species occurs in the upper part of the upper Smithian *Anasibirites multiformis* ammonoid beds in south China (Brayard and Bucher 2008).

Tirolites and *Columbites* are characteristic genera in the early Spathian radiated ammonoid fauna (Tozer 1982; Galfetti et al. 2007). *Tirolites* and *Columbites* beds were reported from south China, Pakistan, Himalayas and USA (Guex 1978; Brayard and Bucher 2008; Balini et al. 2010). In particular, *T. cassianus* is a significant age diagnostic species in the lowermost Spathian in the Tethys (Krystyn 1974, 1978; Posenato 1992). In northeastern Vietnam, the S–S boundary was determined by the first occurrence of *T.* cf. *cassianus* in the middle part of the Bac Thuy Formation (Figs. 3-6).

4.2. Conodont biostratigraphy

In the study area, three conodont zones, *Novispathodus* ex gr. *waageni*, *N.* ex gr. *pingdingshanensis*, and *Icriospathodus collinsoni* were recognized. *N.* ex gr. *waageni* is a characteristic species of Smithian (Tong et al. 2007; Orchard 2010). Generally, the first appearance datum (FAD) of *N.* ex gr. *waageni* (=*N. waageni* sensu lato) was taken as the base of the Olenekian (Lucas and Orchard 2007; Orchard and Krystyn 2007; Krystyn et al. 2007; Zhao et al. 2007; Orchard 2010; Goudemand 2014; Chen et al. 2015). In the Bac Thuy Formation, the *N.* ex gr. *pingdingshanensis* Zone begins with the first occurrence of the nominal species and ends with the first occurrence of *I. collinsoni*.

Typical form of *N. pingdingshanensis*, characterized by a small blade-like element, was described originally by Zhao et al. (2007) from the West Pingdingshan section, Anfui Province, south China, and had been reported from several localities in China (Liang et al. 2011; Ji et al.

2011; Goudemand et al. 2012; Chen et al. 2015). These authors regarded *N.* ex gr. *pingdingshanensis* as a representative of the lower Spathian. However, in the Bac Thuy Formation, *N.* ex gr. *pingdingshanensis* including typical form of *N. pingdingshanensis* are commonly found in the dark gray limestone of the uppermost Smithian *X. variocostatus* ammonoid beds at 1.5 m below the first occurrence of basal Spathian ammonoid *T.* cf. *cassianus* (NT01-07 and KC02-10 in Figs. 2, 6). This association is also known in Guangxi, south China (Goudemand et al. 2012). Apparently, *N.* ex gr. *pingdingshanensis* ranges from the latest Smithian into the earliest Spathian.

The first occurrence of *I. collinsoni* is about 30 cm above the bed characterized by the ammonoid *Tirolites* sp. nov. (Figs. 5, 6). The conodont assemblage of the *I. collinsoni* Zone consists mainly of the name giver, *Novispathodus triangularis*, *I. collinsoni*, and *I. crassatus*. These new conodont taxa appeared at the beginning of the Spathian, which is marked by a tremendous conodont evolutionary radiation (Orchard 2007).

5. Results of carbon isotope and TOC

5.1. Carbon isotope record

Carbon isotope ratios of bulk carbonate from the suites of Bac Thuy Formation samples range between −2.49‰ and 5.74‰ (Table 1). Carbon isotope stratigraphies of the KC02 and NT01 sections are presented in Fig. 7A and B, and the composite carbon isotope stratigraphy of the two sections with biostratigraphy is shown in Fig. 7D.

The carbon isotope values are relatively constant ranging from −2.49 to −0.81‰ in the *N.* ex gr. *waageni* conodont Zone and the *O. koeneni* ammonite beds of the lower and middle part of the Bac Thuy Formation. A prominent steep positive excursion in δ^{13}C with values increasing from around −2.22 to +5.02‰ occurs near the top of *N.* ex gr. *waageni* Zone and into the lower *N.* ex gr. *pingdingshanensis* conodont Zone, which corresponds to the lower to middle *X. variocostatus* ammonoid beds. Following a gentler increasing
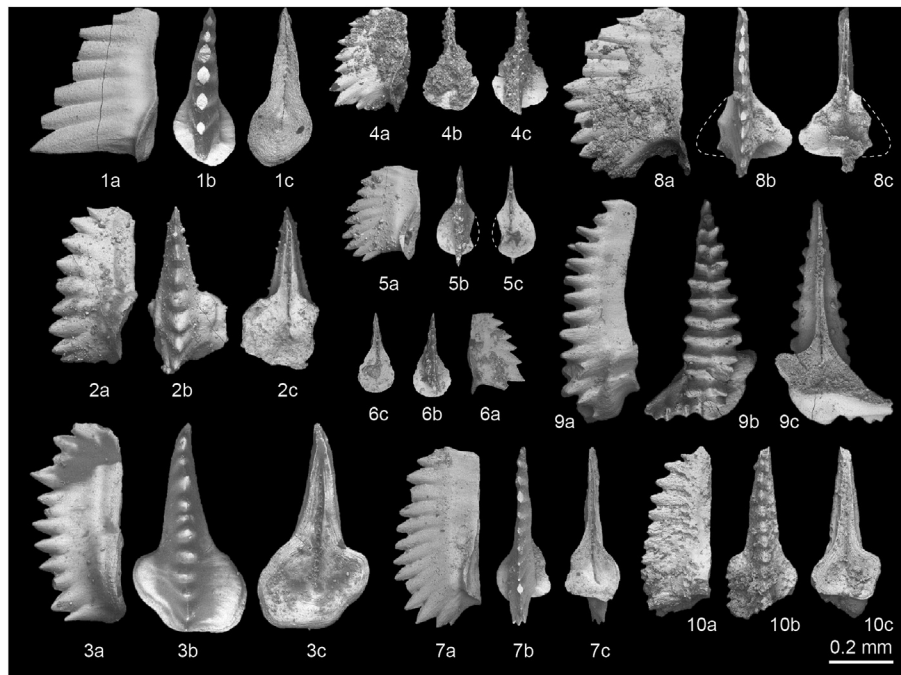
Fig. 5. SEM images of Smithian and Spathian conodonts from the Bac Thuy Formation, Lang Son area, northeastern Vietnam. MPC = Micropaleontology Collection, National Museum of Nature and Science, Tsukuba. Figures "a", "b" and "c" show lateral, upper and lower views of specimens, respectively. 1. *Neospathodus dieneri* Sweet, MPC25277, from KC02-02. 2-3, *Icriospathodus? zaksi* (Buryi). 2, MPC25652, from NT01-07; 3, MPC25651, from KC02-10. 4-5, *Novispathodus* ex gr. *pingdingshanensis* (Zhao & Orchard). 4, MPC25395, from NT01-07; 5, MPC28859, from KC02-10. 6-7, *Novispathodus* ex gr. *abruptus* (Orchard). 6, MPC28856, from KC02-10; 7, MPC25544, from KC02-14. 8, *Novispathodus triangularis* (Bender), MPC25400, from KC02-15. 9, *Icriospathodus collinsoni* (Solien), MPC25635, from KC02-15. 10, *Icriospathodus? crassatus* (Orchard), MPC25684, from KC02-15. All specimens are P₁ element.
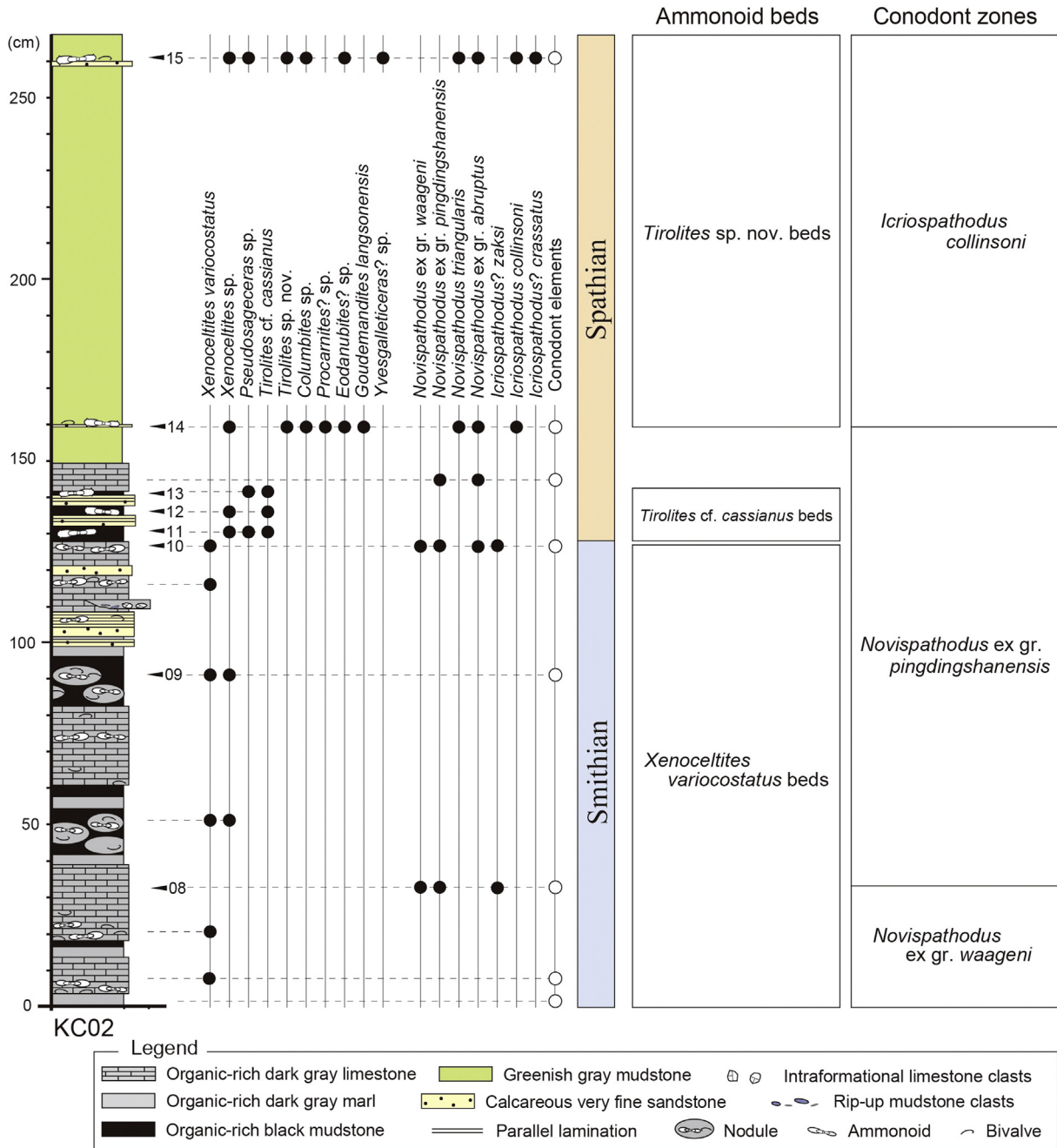
Fig. 6. Detailed columnar section (KC02) embracing the Smithian–Spathian boundary showing ammonoids and conodonts from the organic-rich dark gray limestone and black mudstone of the middle part of the Bac Thuy Formation.

trend in δ¹³C, a gradual δ¹³C decreasing trend is seen in the *N.* ex gr. *pingdinshanesis* conodont Zone. The former interval corresponds to the middle part of *X. variocostatus* ammonite beds, while the latter occurs from the upper *X. variocostatus* through the *T.* cf. *cassianus*, and into the basal *Tirolites* sp. nov. ammonoid beds. The δ¹³C values decrease from around +5.5 to +5.0‰ across the Smithian–Spathian boundary, which was recognized by the first occurrence of *T.* cf. *cassianus* in the Ky Cung River section. In the lower Spathian limestone, δ¹³C became lower with values of 1.3–2.1‰ in the *Tirolites* sp. nov. ammonoid beds.

5.2. Total organic carbon content (TOC)

In the middle Smithian *O. koeneni* ammonoid beds, whitish gray hemipelagic carbonates and greenish gray mudstone intercalating with limestone breccia have TOC ranges from about 0.01 to 0.05 wt%.

The upper Smithian *X. variocostatus* and lower Spathian *T.* cf. *cassianus* ammonoid beds are dominated by organic carbon rich dark gray limestone and mudstone. TOC of lower part of the *X. variocostatus* ammonoid beds ranges from 0.15 to 0.3 wt%, whereas in the upper part of these ammonoid beds and in the overlying *T.* cf. *cassianus* ammonoid beds, they range from approximately 0.3 to 0.9 wt%, with a maximum TOC value of 0.88 wt% in the lower Spathian. In the upper *Tirolites* sp. nov. ammonoid beds composed of hemipelagic greenish gray mudstone intercalating with whitish gray thin bedded carbonates and isolated limestone breccia, TOC ranges from 0.05 to 0.1 wt%.

The organic carbon-rich, dark gray limestone and mudstone are characterized by well-preserved laminations, pyrite aggregates, low-diversity small grazing traces, and monospecific ammonoid, bivalve and ostracod assemblages (Komatsu et al. 2013, 2014a; Shigeta et al. 2014), and are interpreted to be deposited in anoxic to dysoxic marginal
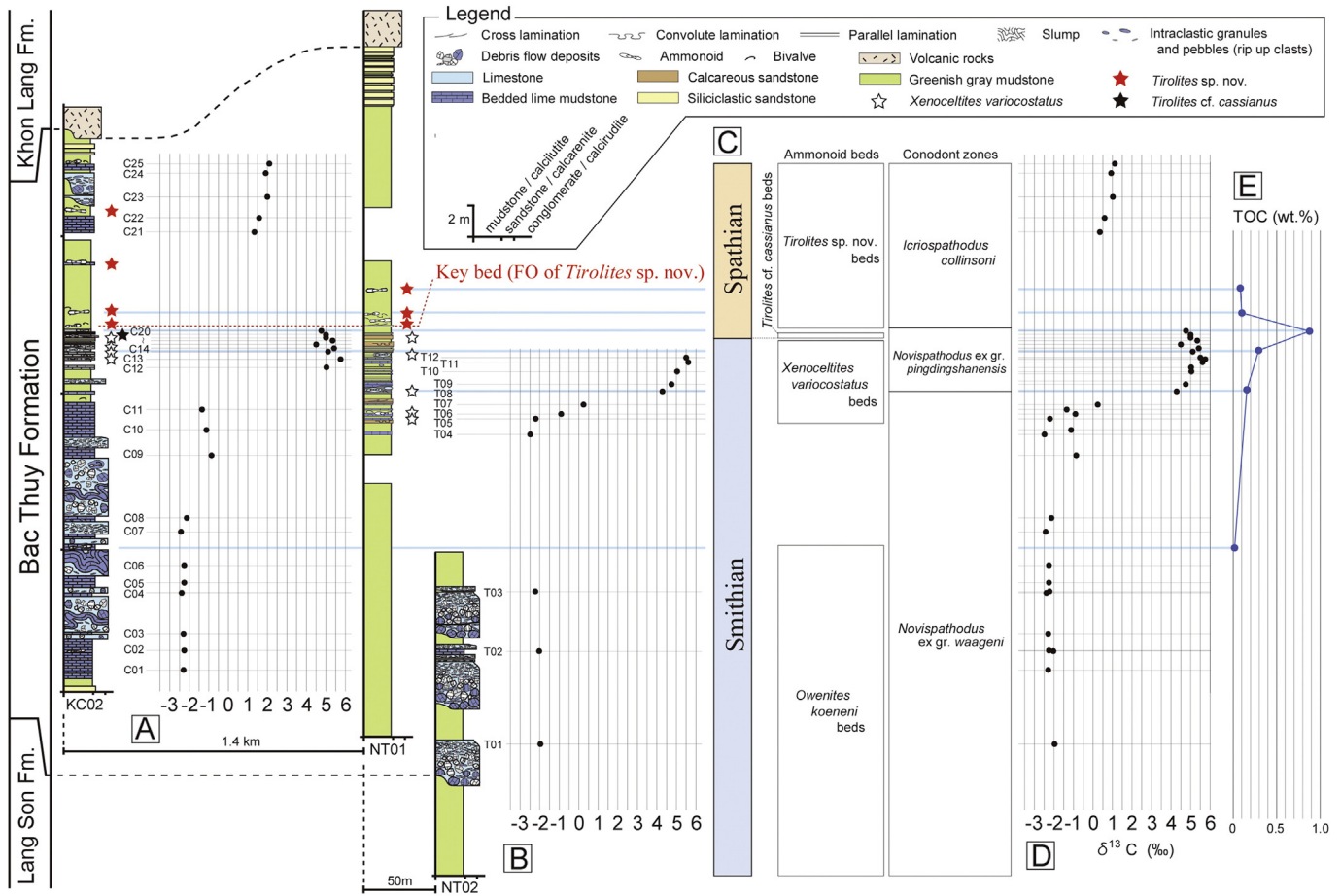
Fig. 7. (A) Carbon isotopic data from KC02. (B) Carbon isotopic data from NT01 and NT02. (C) Composite carbon isotopic curve on the basis of (A) and (B). (D) TOC content profile.

basin plane environments (Komatsu et al. 2013). According to Arthur and Sageman (1994), TOC of the recent anoxic offshore mudstone is usually over 1 wt%. Thus, in the upper part of *X. variocostatus* and *T.* cf. *cassianus* ammonoid beds, organic rich limestone and mudstone characterized by around 1 wt% were probably accumulated in dysoxic to anoxic marginal basin plane environments during the latest Smithian to the earliest Spathian.

6. Discussion

Around the Smithian–Spathian (S–S) boundary, a pronounced positive carbon isotope excursion has been reported from both Tethyan and Boreal marine deposits (Payne et al. 2004; Galfetti et al. 2007; Horacek et al. 2007; Tanner 2010; Liang et al. 2011; Sun et al. 2012; Clarkson et al. 2013; Chen et al. 2016). Payne et al. (2004) reported a composite carbon isotopic curve from the Upper Permian to Upper Triassic in south China, and showed a positive excursion in $\delta^{13}C_{carb}$ with values increasing by around −3.0 to +2.0‰ around the S–S boundary. A prominent positive excursion in $\delta^{13}C$ with values from around −3 to +5‰ was also reported from the North and West Pingdingshan sections, Anhui, south China (Tong et al. 2007). A large positive excursion exceeding 7‰ was reported by Horacek et al. (2007) at the S–S boundary in the Abadeh, Zal and Amo sections, northern and central Iran. In the Boreal realm, an increase in $\delta^{13}C_{org}$ by approximately −33 to −28‰ was observed at the transition of S–S boundary in the Dicksonfjellet section on Spitsbergen (Galfetti et al. 2007).

Liang et al. (2011) provided a detailed intercalibration of conodont biostratigraphy and carbon isotope stratigraphy around the S–S boundary in the West Pingdingshan Section, south China. In their paper, the S–

S boundary was defined by the First Appearance Datum (FAD) of the conodont *N. pingdingshanensis* in the middle part of Bed 52; there, the $\delta^{13}C_{carb}$ value distinctively changes from −2 to +4‰ at that level. Based on the Vietnamese ammonoid and conodont biostratigraphic data of this paper, this positive excursion in $\delta^{13}C$ appears to peak in the uppermost Smithian.

Positive major $\delta^{13}C$ excursions are often associated with the accumulation of black organic-rich deposits (ex. Kump 1999; Buggisch and Joachimski 2006; Takashima et al. 2009; Komatsu et al. 2014b; Sun et al. 2015). Around the S–S boundary, a positive excursion of $\delta^{13}C$ is observed in the organic carbon-rich black shale (Galfetti et al. 2008; Komatsu et al. 2014a). According to Galfetti et al. (2008), in Guangxi Province, south China, the "*Xenoceltites* beds" in the top part of Unit IV of the Luolou Formation are characterized by pyrite aggregates and laminated organic-rich limestone and shale devoid of bioturbation, which suggests low-energy depositional environments and some environmental stress such as oxygen deficiency. Moreover, a positive major $\delta^{13}C$ excursion is recorded in the "*Xenoceltites* ammonoid beds". In the section NT01 of our study area, the positive excursion in $\delta^{13}C$ clearly coincides with the deposition of alternating dark gray organic-rich limestone and mudstone showing high TOC value (0.88 wt%) in the latest Smithian *X. variocostatus* Beds of the Bac Thuy Formation. These organic-rich deposits were accumulated in the latest Smithian to earliest Spathian marginal basin environments under an oxygen-deficient condition (Komatsu et al. 2014a; Shigeta et al. 2014). Recently, Tian et al. (2014) studied long-term changes in marine redox conditions in the Nanpanjiang Basin on the South China Block on the basis of pyrite framboid size distributions, and reported oxygen-poor conditions were expanded during the late Smithian to early Spathian. Sun et al. (2015) also reported minute

pyrite framboids in detail from the Black Shale Unit equivalent to *Parachirognathus–Pachycladina* and *N. pingdingshanensis* conodont zones in the Nanpanjiang Basin, which reveals widespread anoxia during the latest Smithian to earliest Spathian. Sun et al. (2012) analyzed oxygen isotopes of conodont apatite ($\delta^{18}O_{apatite}$) from sections in south China, and reported that high temperature of seawater, possibly exceeding 40 °C, was marked in the latest Smithian. Saito et al. (2013) demonstrated that, based on biomarker analysis, upwelling and marine productivity increased during the S–S boundary in south China. Therefore, it is plausible to consider that the positive $\delta^{13}C$ excursion in the latest Smithian is strongly related to increased primary productivity and organic carbon accumulation which resulted in global expansion of anoxia. However, in the major oceanic anoxic events such as the Devonian Kelwasser Events, Devonian Hangenberg Event, and Cretaceous OAE 1a and 2, positive carbon isotope excursions of carbonate are about 2–4‰ (e.g., Buggisch and Joachimski 2006; Jarvis et al. 2006; Jenkyns 2010; Kuhnt et al. 2011). Since total 8‰ positive shift in $\delta^{13}C_{carb}$ at the S–S boundary is 2–3 times larger than that of the major oceanic anoxic events, much greater burial of organic carbon is needed to account for such large positive excursion at the S–S boundary.

7. Conclusions

In the Olenekian Bac Thuy Formation, the positive excursion of $\delta^{13}C$ was recognized in the upper Smithian *X. variocostatus* ammonoid beds, and the $\delta^{13}C$ values decrease across the Smithian–Spathian boundary defined by a first occurrence of *T.* cf. *cassianus*. High $\delta^{13}C$ values around +5.5 to +5.8‰ are recorded in the organic rich limestone and mudstone characterized by high TOC value, which are thought to have accumulated in dysoxic to anoxic conditions. Such a positive excursion may attribute to global expansion of marine anoxia and massive accumulation of organic carbon at the S–S boundary in the Early Triassic global warming. The latest Smithian positive excursion of $\delta^{13}C$ is useful for the global correlation.

8. Systematic paleontology

Important age diagnostic conodonts are shown in Fig. 5. Two conodont species of genus *Novispathodus* are remarked here. The other species already described in Shigeta et al. (2014). All specimens are stored in the National Museum of Nature and Science.

Genus *Novispathodus* Orchard 2005

Novispathodus ex gr. *abruptus* (Orchard 1995)

(Figs. 5–6a–c, 7a–c)

1981 *Neospathodus homeri* (Bender)-Koike, pl. 1, Fig. 5

1995 *Neospathodus abruptus* Orchard, p. 118–119, Figs. 3.16–3.19, 3.23–3.26

2005 multielement apparatus of *Novispathodus abruptus* (Orchard)-Orchard, p. 90–91, Text-fig. 16

2007 *Novispathodus abruptus* (Orchard)-Lucus and Orchard, Figs. 7.10–7.12

2011 *Neospathodus abruptus* Orchard-Ji et al., Fig. 3.8

2014 *Triassospathodus homeri* (Bender)-Maekawa and Igo, p. 253–254, Figs. 181.43–181.48

2014 *Triassospathodus symmetricus* (Orchard)-Maekawa and Igo in Shigeta, p. 254, Figs. 182–185, 186.1–186.3

2015 *Novispathodus abruptus* (Orchard)-Chen et al., Figs. 7.14, 7.18, 8.2, 9.13, 9.16, 9.17

2015 *Triassospathodus homeri* (Bender)-Chen et al., Figs. 7.13, 8.18, 9.14, 9.19

2015 *Triassospathodus symmetricus* (Orchard)-Chen et al., Figs. 8.1, 8.19

Material examined: Three specimens, MPC28856–28858, from KC02-10, two specimens, MPC25542, 25543, from KC02-12, three specimens, MPC25544–25546, from KC02-14, and forty-five specimens, MPC25540, 25541, 25547–25589, from KC02-15.

Original diagnosis: A species in which segminate elements representing small to medium growth stages are relatively short and high with a length:height ratio of about 1.5:1, and up to about 12 upright to reclined denticles that increase in height toward the posterior except for the terminal 1–3 progressively smaller denticles that descend rapidly to the posterior tip of the blade. Large specimens are subrectangular in lateral view with a blade ratio of 2–2.5, and up to 16 denticles that are of subequal height in the central part of the element; the lower posterior denticles may fuse to form a thicker cusp. The lower margin of the basal cavity is irregularly oval to subcircular in outline, with slight elongation beneath the denticles on the posterior margin (Orchard 1995).

Remarks: Vietnamese specimens show subrectangular lateral form with fused and posteriorly reclined denticles which number is from 10 to 18 (average 13). This feature is similar to large specimen of *N. abruptus* (Orchard 1995). Some specimens show secondary characters; strongly downturned posterior part of basal cavity, subtriangular or cordiform basal cavity, laterally expanded robust element with node-like denticles. These characters indicate morphological variation in the species. Particularly, posteriorly downturned elements (Shigeta et al. 2014, figs. 182.34–182.36, 185.27–185.32, etc.) and expanded robust elements (Shigeta et al. 2014, figs. 184.22–184.24, 185.33–185.35, etc.) show large differences from the holotype (Orchard 1995, figs. 3.23–3.24). It indicates that *N. abruptus* from the Bac Thuy Formation contains three morphotypes (typical form, posterior downturned form and expanded robust form) at least. Several specimens are very similar to *T. symmetricus* (Orchard 1995), but the species is distinguished from *N. abruptus* by slightly fewer, strongly inclined and sharp pointed denticles which number is slightly fewer.

Occurrence: KC02-10, KC02-12–KC02-15 in the Bac Thuy Formation within the portion of *N.* ex gr. *pingdingshanensis* Zone and *I. collinsoni* Zone that include the uppermost part of *X. variocostatus* beds, *T.* cf. *cassianus* beds and a part of *Tirolites* sp. nov. beds.

Novispathodus ex gr. *pingdingshanensis* (Zhao and Orchard 2007)

(Figs. 5–4a–c, 5a–c)

2007 *Neospathodus pingdingshanensis* Zhao and Orchard, p. 36, pl. 1, Figs. 4A–4C

2012 *Novispathodus pingdingshanensis* (Zhao and Orchard)-Goudemand and Orchard, in Goudemand et al., p. 1030–1031, Figs. 2B, F, G, I-J, M, P, Q, AD, 3T-U, 6

2014 *Novispathodus pingdingshanensis* (Zhao and Orchard)-Maekawa and Igo in Shigeta, p. 239–240, Figs. 171.13–171.31

2015 *Novispathodus pingdingshanensis* (Zhao and Orchard)-Chen et al., Figs. 7.3, 8.5, 8.6

Material examined: One specimen, MPC25391, from KC02-08, two specimens, MPC25392 and 28859, from KC02-10, one specimen, MPC25393, from KC02-12, one specimen, MPC25394, from KC02-17, and two specimens, MPC25395, 25396, from NT01-07.

Original diagnosis: Small segminate elements characterized by a length:height ratio in the range of 1.32–2.34, and about 4–9 robust, wide and mostly fused denticles. In lateral view, the basal margin is straight. A large, broadly expanded oval to subrounded basal cavity is upturned on the inner margin and flat to downturned on the outer margin (Zhao et al. 2007).

Remarks: Goudemand et al. (2012) reported conodont assemblages from Smithian–Spathian boundary sections in south China which contains some specimens of *N. pingdingshanensis* whose basal margin is non-straight and posterior margin is upturned. Vietnamese specimens (Fig. 5–4a–c, 5–5a–c; Maekawa and Igo 2014 in Shigeta et al. 2014, figs. 171.13–171.16, 171.19–171.21) and south China specimens (Goudemand et al. 2012, figs. 2F, 2J) show the cusp which bears 2–5 posterior small denticles. And also some specimens (Ji et al., 2011, fig. 7; Goudemand et al. 2012, figs. 2B, C; Maekawa and Igo 2014, figs. 171.17, 171.18) have large basal cavity which length is

two-thirds of element length. These forms show intraspecific variants of *N. pingdingshaensis*. Denticulation of some specimens slightly weak inclined posteriorly than typical specimens, but lateral form of element and subrounded basal cavity are similar to holotype (e.g. Goudemand et al. 2012, figs. 2B, C). The fact indicates that Vietnamese specimen (Figs. 5–5a–c) fall within morphological variation of *N. pingdingshanensis* sensu lato.

Occurrence: KC02-08, KC02-10, KC02-12, KC02-17, and NT01-07 in the Bac Thuy Formation within the *N.* ex gr. *pingdingshanensis* Zone that includes *X. variocostatus* beds and *T.* cf. *cassianus* beds. Typical forms of *N. pingdingshanensis* occur from KC02-10 and NT01-07 (Figs. 4, 5).

Acknowledgements

References

Algeo, T.J., Chen, Z.Q., Fraiser, M.L., Twitchett, R.J., 2011. Terrestrial–marine teleconnections in the collapse and rebuilding of Early Triassic marine ecosystems. Palaeogeogr. Palaeoclimatol. Palaeoecol. 308, 1–11.

Arthur, M.A., Sageman, B.B., 1994. Marine black shales: depositional mechanisms and environments of ancient deposits. Annu. Rev. Earth Planet. Sci. 22, 499–551.

Balini, M., Lucas, S.G., Jenks, J.F., Spielmann, J.A., 2010. Triassic ammonoid biostratigraphy: an overview. In: Lucas, S.G. (Ed.), The Triassic TimescaleGeological Society Special Publication Vol. 334. Geological Society of London, London, pp. 221–262.

Brayard, A., Bucher, H., 2008. Smithian (Early Triassic) ammonoid faunas from northwestern Guangxi (South China): taxonomy and biochronology. Fossils Strata 55, 1–179.

Buggisch, W., Joachimski, M.M., 2006. Carbon isotope stratigraphy of the Devonian of Central and Southern Europe. Palaeogeogr. Palaeoclimatol. Palaeoecol. 240, 68–88.

Chen, Y.L., Jiang, H.S., Richoz, S., Yan, C.B., Lai, X.L., Sun, Y.D., Liu, X.D., Wang, L.N., 2015. Early Triassic conodonts of Jiarong, Nanpanjiang Basin, southern Guizhou Province, South China. J. Asian Earth Sci. 105, 104–121.

Chen, Y.L., Kolar-Jurkovšek, T., Jurkovšek, B., Aljinović, D., Richoz, S., 2016. Early Triassic conodonts and carbonate carbon isotope record of the Idrija–Žiri area, Slovenia. Palaeogeogr. Palaeoclimatol. Palaeoecol. 444, 84–100.

Chen, Y.L., Twitchett, R.J., Jiang, H.S., Richoz, S., Lai, X.L., Yan, C.B., Sun, Y.D., Liu, X.D., Wang, L.N., 2013. Size variation of conodonts during the Smithian–Spathian (Early Triassic) global warming event. Geology 41, 823–826.

Clarkson, M.O., Richoz, S., Wood, R.A., Maurer, F., Krystyn, L., McGurty, D.J., Astratti, D., 2013. A new high-resolution δ13C record for the Early Triassic: insights from the Arabian Platform. Gondwana Res. 24, 233–242.

Dang, T.H., 2006. Mesozoic. In: Thanh, T.D. (Ed.), Stratigraphic Units of Vietnam. Vietnam National University Publishing House, Hanoi, pp. 245–366.

Dang, T.H., Nguyen, D.H., 2005. Fossil zones and stratigraphic correlation of the Lower Triassic sediments of East Bac Bo. J. Geol. Ser. A 11-12, 1–9.

Enos, P., Lehrmann, D.J., Jiayong, W., Youyi, Y., Jiafei, X., Chaikin, D.H., Minzoni, M., Berry, A.K., Montgomery, P., 2006. Triassic evolution of the Yangtze Platform in Guizhou Province, People's Republic of China. The Geological Society of America, Special Paper 417. Geological Society of America, Boulder, Colorado (105 pp.).

Galfetti, T., Bucher, H., Martini, R., Hochuli, P.A., Weissert, H., Crasquin-Soleau, S., Brayard, A., Goudemand, N., Bruhwiler, T., Guodun, K., 2008. Evolution of Early Triassic outer platform paleoenvironments in the Nanpanjiang Basin (South China) and their significance for the biotic recovery. Sediment. Geol. 204, 36–60.

Galfetti, T., Hochuli, P.A., Brayard, A., Bucher, H., Weissert, H., Vigran, J.O., 2007. Smithian–Spathian boundary event: evidence for global climatic change in the wake of the end-Permian biotic crisis. Geology 35, 291–294.

Goudemand, N., 2014. Note on the conodonts from the Induan–Olenekian boundary. Albertiana 42, 49–51.

Goudemand, N., Orchard, M.J., Tafforeau, P., Urdy, S., Brühwiler, T., Brayard, A., Galfetti, T., Bucher, H., 2012. Early Triassic conodont clusters from South China: revision of the Architecture of the 15 element apparatuses of the superfamily Gondolellidae. Palaeontology 55, 1021–1034.

Guex, J., 1978. Le Trias inférieur des Salt Ranges (Pakistan): problèmes biochronologiques. Eclogae Geol. Helv. 71, 105–141.

Horacek, M., Richoz, S., Brandner, R., Krystyn, L., Spötl, C., 2007. Evidence for recurrent changes in Lower Triassic oceanic circulation of the Tethys: the δ13C record from marine sections in Iran. Palaeogeogr. Palaeoclimatol. Palaeoecol. 252, 355–369.

Jarvis, I., Gale, A.S., Jenkyns, H.C., Pearce, M.A., 2006. Secular variation in Late Cretaceous carbon isotopes: a new δ13C carbonate reference curve for the Cenomanian–Campanian (99.6–70.6 Ma). Geol. Mag. 143, 561–608.

Jenkyns, H.C., 2010. Geochemistry of ocenic anoxic events. Geochem. Geophys. Geosyst. 11, Q03004. http://dx.doi.org/10.1029/2009GC002788.

Ji, W., Tong, J., Zhao, L., Zhuo, S., Chen, J., 2011. Lower-Middle Triassic conodont biostratigraphy of the Qingyan section, Guizhou Province, Southwest China. Palaeogeogr. Palaeoclimatol. Palaeoecol. 308, 213–223.

Kiparisova, L.D., Popov, Y.N., 1956. Subdivision of the Lower series of the Triassic System into stages. Dokl. Akad. Nauk USSR Ser. Geol. 109, 842–845.

Koike, T., 1981. Biostratigraphy of Triassic Conodonts in Japan. Science Reports of the Yokohama National University Section II. Biological and Geological Sciences Vol. 28, pp. 25–46 (pl. 1-2).

Komatsu, T., Dang, T.H., 2007. Lower Triassic bivalve fossils from the Song Da and An Chau Basins, North Vietnam. Paleontol. Res. 11, 135–144.

Komatsu, T., Kato, S., Hirata, K., Takashima, R., Ogata, Y., Oba, M., Naruse, H., Ta, P.H., Nguyen, D.P., Dang, T.H., Doan, N.T., Nguyen, H.H., Sakata, S., Kaiho, K., Königshof, P., 2014b. Devonian–Carboniferous transition containing a Hangenberg Black Shale equivalent in the Pho Han Formation on Cat Ba Island, northeastern Vietnam. Palaeogeogr. Palaeoclimatol. Palaeoecol. 404, 30–43.

Komatsu, T., Naruse, H., Shigeta, Y., Takashima, R., Maekawa, T., Dang, T.H., Dinh, C.T., Nguyen, D.P., Nguyen, H.H., Tanaka, G., Sone, M., 2014a. Lower Triassic mixed carbonate and siliciclastic setting with Smithian–Spathian anoxic to dysoxic facies, An Chau basin, northeastern Vietnam. Sediment. Geol. 300, 28–48.

Komatsu, T., Shigeta, Y., Dang, T.H., Nguyen, D.H., Dinh, C.T., Maekawa, T., Tanaka, G., 2013. *Crittendenia* (Bivalvia) from the Lower Triassic Olenekian Bac Thuy Formation, An Chau Basin, Northern Vietnam. Paleontol. Res. 17, 1–11.

Krystyn, L., 1974. Die Tirolites-Fauna (Ammonoidea) der untertriassischen Werfener Schichten Europas und ihre stratigraphische Bedeutung. Sitzungsberichten der Österreichische Akademie Wissenschaften. Mathematisch-naturwissenschaftlichen Klasse, Abt. 1 Vol. 183, pp. 29–50.

Krystyn, L., 1978. Eine neue Zonengliederung im alpinmediterranean Unterkarn. In: Zapfe, H. (Ed.), Beiträge zur Biostratigraphie der Tethys-Trias. Schriftenreihe Erdwissenschaftlichen Kommissionen Osterreichische Akademie der Wissenschaften Vol. 4, pp. 37–75.

Krystyn, L., Richoz, S., Bhargava, N.O., 2007. The Induan–Olenekian Boundary (IOB) in Mud — an update of the candidate GSSP section M04. Albertiana 36, 33–49.

Kuhnt, W., Holbourn, A., Moullade, M., 2011. Transient global cooling at the onset of early Aptian oceanic anoxic event (OAE) 1a. Geology 39, 323–326.

Kump, L.R., 1999. Interpreting carbon-isotope excursions: strangelove oceans. Geology 19, 299–302.

Lehrmann, D.J., Donghong, P., Enos, P., Minzoni, M., Ellwood, B.B., Orchard, M.J., Jiyan, Z., Jiayong, W., Dillett, P., Koenig, J., Steffen, K., Druke, D., Druke, J., Kessel, B., Newkirk, T., 2007b. Impact of differential tectonic subsidence on isolated carbonate-platform evolution: Triassic of the Nanpanjiang Basin, south China. Am. Assoc. Pet. Geol. Bull. 91, 287–320.

Lehrmann, D.J., Payne, J.L., Pei, D., Enos, P., Druke, D., Steffen, K., Zhang, J., Wei, J., Orchard, M.J., Ellwood, B., 2007a. Record of the end-Permian extinction and Triassic biotic recovery in the Chongzuo-Pingguo platform, southern Nanpanjiang basin, Guangxi, south China. Palaeogeogr. Palaeoclimatol. 252, 200–217.

Liang, D., Tong, J.N., Zhao, L.S., 2011. Lower Triassic Smithian–Spathian Boundary at West Pingdingshan Section in Chaohu, Anhui Province. Sci. China Earth Sci. 54, 372–379.

Lucas, S.G., Orchard, M.J., 2007. Triassic lithostratigraphy and biostratigraphy North of Currie, Elko Country, Nevada. N. M. Mus. Nat. Hist. Sci. Bull. 40, 119–126.

Maekawa, T., Igo, H., 2014. Conodonts. In: Shigeta, Y., Komatsu, T., Maekawa, T., Dang, T.H. (Eds.), Olenekian (Early Triassic) Stratigraphy and Fossil Assemblages in Northeastern VietnamNational Museum of Nature and Science Monographs No. 45. National Museum of Nature and Science, Tokyo, pp. 190–271 (Tokyo).

Maekawa, T., Komatsu, T., Shigeta, Y., Dang, T.H., Dinh, C.T., 2015. First occurrence of Early Triassic conodonts from the Lang Son Formation, northeastern Vietnam. Paleontol. Res. 19, 312–320.

Maekawa, T., Komatsu, T., Shigeta, Y., Dang, T.H., Nguyen, D.P., 2016. Upper Induan and Lower Olenekian conodont assemblages from the lowest part of the Bac Thuy Formation in the Ban Ru area, Northeastern Vietnam. In: Phan, K.L., Pham, V.L., Luu, D.C., Nguyen, T.M., Tran, V.Y., Dinh, T.P., Tran, T.H., Nguyen, Q.B., Vu, V.L., Tran, T.H.A., Pham, H.T., Nguyen, T.T. (Eds.), Proceedings of the 2nd National Scientific Conference of Vietnam Natural Museum System. Publishing House for Science and Technology, Hanoi, pp. 193–207.

Ogg, J.G., 2012. Triassic. In: Gradstein, F.M., Ogg, J.G., Schmitz, M.D., Ogg, G.M. (Eds.), The Geologic Time Scale vol. 2. Elsevier, Amsterdam, pp. 681–730.

Orchard, M.J., 1995. Taxonomy and correlation of Lower Triassic (Spathian) segminate conodonts from Oman and revision of some species of *Neospathodus*. J. Paleontol. 69, 110–122.

Orchard, M.J., 2005. Multielement conodont apparatuses of Triassic Gondolelloidea. Spec. Pap. Palaeontol. 73, 73–101.

Orchard, M.J., 2007. Conodont diversity and evolution through the latest Permian and Early Triassic upheavals. Palaeogeogr. Palaeoclimatol. Palaeoecol. 252, 93–117.

Orchard, M.J., 2010. Triassic conodonts and their role in stage boundary definition. In: Lucas, S.G. (Ed.), The Triassic Timescale. Geological Society, London, Special Publications Vol. 334, pp. 139–161.

Orchard, M.J., Krystyn, L., 2007. Conodont from the Induan–Olenekian boundary interval at Mud Spiti. Albertiana 35, 30–34.

Payne, J.L., Clapham, M.E., 2012. End-Permian mass extinction in the oceans: an ancient analog for the twenty-first century. Annu. Rev. Earth Planet. Sci. 40, 89–111.

Payne, J.L., Lehrmann, D.J., Summers, M., Wei, J.Y., Orchard, M.J., Schrag, D.P., Knoll, A.H., 2004. Large perturbations of the carbon cycle during recovery from the end-Permian extinction. Science 305, 506–509.

Posenato, R., 1992. Tirolites (Ammonoidea) from the Dolomites, Bakony and Dalmatia: taxonomy and biostratigraphy. Eclogae Geol. Helv. 85, 893–929.

Saito, R., Kaiho, K., Oba, M., Takahashi, S., Chen, Z.-Q., Ong, J., 2013. A terrestrial vegetation turnover in the middle of the Early Triassic. Glob. Planet. Chang. 105, 152–159.

Shigeta, Y., Komatsu, T., Maekawa, T., Dang, T.H., 2014. Olenekian (Early Triassic) Stratigraphy and Fossil Assemblages in Northeastern Vietnam. National Museum of Nature and Science, Monographs Vol. 45. National Museum of Nature and Science, Tokyo (309 pp.).

Song, H., Wignall, P.B., Tong, J., Bond, D.P.G., Song, H., Lai, X., Zhang, K., Wang, H., Chen, Y., 2012. Geochemical evidence from bio-apatite for multiple oceanic anoxic events during Permian–Triassic transition and the link with end-Permian extinction and recovery. Earth Planet. Sci. Lett. 353-354, 12–21.

Stanley, S.M., 2009. Evidence from ammonoids and conodonts for multiple Early Triassic mass extinction. Proc. Natl. Acad. Sci. U. S. A. 106, 15264–15267.

Sun, Y.D., Joachimski, M.M., Wignall, P.B., Yan, C.B., Chen, Y.L., Jiang, H.S., Wang, L.N., Lai, X.L., 2012. Lethally hot temperatures during the Early Triassic greenhouse. Science 338, 366–370.

Sun, Y.D., Wignall, P.B., Joachimski, M.M., Bond, D.P.G., Grasby, S.E., Sun, S., Yan, C.B., Wang, L.N., Chen, Y.L., Lai, X.L., 2015. High amplitude redox changes in the late early Triassic of South China and the Smithian/Spathian extinction. Palaeogeogr. Palaeoclimatol. Palaeoecol. 427, 62–78.

Takashima, R., Nishi, H., Hayashi, K., Okada, H., Kawahata, H., Yamanaka, T., Fernanndo, A., Mampuku, M., 2009. Litho-, bio- and chemostratigraphy across the Cenomanian/ Turonian boundary (OAE 2) in the Vocontian Basin of southeastern France. Palaeogeogr. Palaeoclimatol. Palaeoecol. 273, 61–74.

Tanner, L.H., 2010. The Triassic isotope record. In: Lucas, S.G. (Ed.), The Triassic TimescaleGeological Society Special Publication Vol. 334. Geological Society of London, London, pp. 103–118 (London).

Tian, L., Tong, J.N., Algeo, T.J., Song, H.J., Song, H.Y., Chu, D.L., Shi, L., Bottjer, D.J., 2014. Reconstruction of early Triassic Ocean redox conditions based on framboidal pyrite from the Nanpanjiang Basin, South China. Palaeogeogr. Palaeoclimatol. Palaeoecol. 412, 68–79.

Tong, J.N., Zuo, J.X., Chen, Z.Q., 2007. Early Triassic carbon isotope excursions from South China: proxies for devastation and restoration of marine ecosystems following the end-Permian mass extinction. Geol. J. 42, 371–389.

Tozer, E.T., 1982. Marine Triassic faunas of North America: their significance for assessing plate and terrane movements. Geol. Rundsch. 71, 1077–1104.

Zhao, L, Orchard, M.J., Tong, J., Sun, Z., Zuo, J., Zhang, S., Yun, A., 2007. Lower Triassic conodont sequence in Chaohu, Anhui Province, China and its global correlation. Palaeogeogr. Palaeoclimatol. Palaeoecol. 252, 24–38.